Effect of Gd3+ doping on key structural, morphological, optical, and electrical properties of CdO thin films fabricated by spray pyrolysis using perfume atomizer

8 authors, including:

M. Ravikumar
Arumugam Pillai Seethai Ammal College
5 PUBLICATIONS **8** CITATIONS

SEE PROFILE

Rathinam Chandramohan
Sree Sevugan Annamalai College
149 PUBLICATIONS **1,125** CITATIONS

SEE PROFILE

K. Deva Arun Kumar
Arul Anandar College
21 PUBLICATIONS **56** CITATIONS

SEE PROFILE

S. Valanarasu
Arul Anandar College
75 PUBLICATIONS **361** CITATIONS

SEE PROFILE

Some of the authors of this publication are also working on these related projects:

studying signals of certain biomarkers using living stains View project

MRAC for General Aviation Aircraft View project

CrossMark

Effect of Gd^{3+} doping on key structural, morphological, optical, and electrical properties of CdO thin films fabricated by spray pyrolysis using perfume atomizer

M. Ravikumar[1] · R. Chandramohan[2] · K. Deva Arun Kumar[3] · S. Valanarasu[3] · A. Kathalingam[4] · V. Ganesh[5] · Mohd Shkir ⓘ [5] · S. AlFaify[5]

Abstract Gadolinium-doped cadmium oxide (CdO) thin films were fabricated by spray pyrolysis technique using a perfume atomizer on the glass and silicon substrates at 350 °C. The effect of increasing Gd concentration on the electrical, morphological, optical, and structural properties of deposited films was analyzed. Structural analysis of the pristine and doped CdO thin films showed cubic structures with preferred orientation of (200) direction. The estimated crystallite values ranged from 15 to 21 nm. The structural parameters like dislocation density, microstrain, a number of crystallites per unit area, and texture coefficient were also studied. Scanning electron microscope (SEM) images showed uniformly oriented and cauliflower-like nanostructures grown on the glass substrate for 3at.%-doped CdO films. The doped films' optical transmittance is found to be initially increased and systematically decreased with respect to doping concentrations. The band gap value is in the range of 2.42–2.30 eV for various Gd-doping concentrations (0, 1, 3, and 5%), respectively. The photoluminescence spectra (PL) of films were studied at room temperature and confirms the visible and green emission' peaks are at wavelength 463 and 528 nm, respectively. From the Hall Effect studies, it proved that all the CdO films belong to an n-type degenerate semiconductor, and the low electrical resistivity value was around $3.64 \times 10^{-4} \, \Omega \, \text{cm}$. The n-CdO/p-Si structure with different doping concentrations was subjected to photoconductivity studies and found that it is the maximum of 3% Gd concentration. Higher values of photo responsivity and quantum efficiency was found ~365 mA/W and ~76.64%, respectively, for 3at.% Gd-doped CdO films.
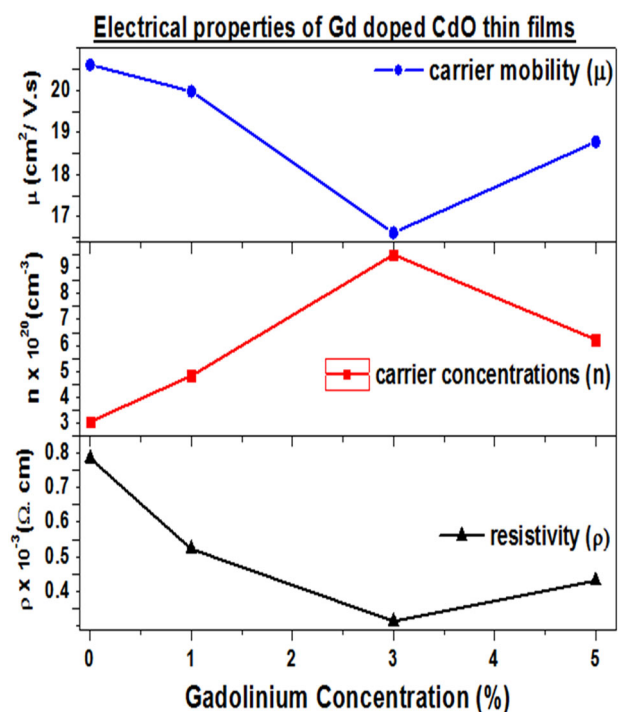
✉ Mohd Shkir
   shkirphysics@gmail.com

[1] Department of Physics, Arumugam Pillai Seethai Ammal College, Tiruppattur 630211, India

[2] Department of Physics, Sree Sevugan Annamalai College, Devakottai 630303, India

[3] PG and Research Department of Physics, Arul Anandar College, Karumathur 625514, India

[4] Millimeter-Wave Innovation Technology Research Center (MINT), Dongguk University-Seoul, Seoul 04620, Republic of Korea

[5] Advanced Functional Materials & Optoelectronic Laboratory (AFMOL), Department of Physics, Faculty of Science, King Khalid University, P.O. Box 9004, Abha 61413, Saudi Arabia

Graphical abstract

Springer

1 Introduction

Nanometer-sized semiconductors have unique physical properties, and in recent years they are studied by different workers with a considerable attention. Moreover, their electrical and optical properties are distinct from that of the bulk counterpart, thereby offering new possible potential applications in many fields [1]. Cadmium oxide (CdO) has high optical transmittance and electrical conductivity at room temperature [2]. This property makes CdO a useful material for various optoelectronic applications like solar cells, optical communication system, smart windows, photo-transistors, and flat-panel displays. It is also found to be useful in other applications such as photodiodes, infrared heat mirror, thin film resistors, and gas sensors [3]. CdO is an n-type degenerate semiconductor with non-stoichiometric composition. The reason is may be due to the presence of either oxygen vacancies or cadmium interstitial. They act as doubly charged donors [4]. CdO is widely studied as an n-type semiconducting metal oxide with the low electrical resistivity [5] and with the band gap of 2.2–2.8 eV [6]. Different authors studied the optoelectronic properties of CdO doping with various metallic ions like: Indium [7], Aluminum [8], Gallium [9], and Manganese [10]. Recently, the effect of Gd and co-doped Ce on the physical properties of CdO thin films were reported by Gupta et al. [11], Dakhel et al. [12], and Pan et al. [13]. In these reports, the Gd-doped films were prepared using pulse laser deposition, sol–gel technique, and RF magnetron sputtering, and their structural, optical, and electrical properties were studied. However, there is still lack of systematic study along with electrical and device making parameters. Many techniques were developed for the deposition of undoped and doped CdO thin films on different substrates like: glass, silicon, etc. by SILAR method [14], CBD [15], sol–gel [12, 16], sputtering [13, 17], and spray pyrolysis [18], etc. Among the different deposition techniques, spray pyrolysis, which is economical, is highly feasible for large area deposition and producing uniform homogenous particle composition, as well-adherent thin films is of interest to researchers [19]. In this spray pyrolysis method, a new class of spray pyrolysis technique of perfume atomizer is found to be suitable for large area deposition of the films and the controlling of various critical deposition parameters like: substrate temperature spray rate, dopant concentration, and substrate-to-nozzle distance [20]. Further, this method was also found more advantageous than the conventional spray pyrolysis method to maintain the good thickness uniformity over a large area and homogenous particle composition with controlled particle size. As per the available literature, there is no report on the fabrication of Gd-doped CdO thin films using spray pyrolysis technique using perfume atomizer. Hence, herein our main aim is to fabricate and investigate the effect of rare earth metal ion (Gd)-doped CdO thin films by the above-mentioned technique; different concentrations of Gd-doped CdO thin films were fabricated on glass and Si substrates, and the heterojunction device was constructed. The effect of varying the Gd concentration on key properties of n-CdO/p-Si heterojunction photodiode was studied. Furthermore, light-dependent electrical measurements like rectification behavior, ideality factor, and barrier height of P–N junction-like structure were also carried out, and the results are discussed in their respective sections.

2 Experimental procedures

2.1 Film preparation

Through spray pyrolysis, using simple perfume atomizer, Gadolinium-doped CdO thin films were prepared. 0.1 M Cadmium acetate dihydrate [Cd $(CH_3COO)_2.2H_2O$] and Gadolinium (III) nitrate hexahydrate (0, 1, 3, and 5%) that were purchased from Sigma-Aldrich was dissolved in 25 ml of de-ionized water at room temperature. This prepared solution was stirred using a magnetic stirrer at room temperature for 15 min until a clear and transparent solution was obtained. The glass substrates were cleaned for 30 min using the detergent solution and de-ionized water, after which they were also cleaned by ultrasonic cleaning in an ultrasonic bath for 10 min. Finally, to complete the cleaning process, all the glass substrates were dried in hot air oven. During the deposition process, the nozzle was kept at a distance of 30 cm from the substrate, and the substrate temperature was maintained at 350 °C. The precursor solution was intermittently sprayed on the preheated substrates with the use of a perfume atomizer. The precursor, when sprayed over the hot substrates pyrolytic decomposes, resulting an orange colored films of CdO. The thickness of all the deposited films was measured by using an Alpha step scan system and tabulated in Table 1.

2.2 Film characterization

The structural analysis was carried out using X-ray diffractometer (PAnalyticalX'Pert) using Cu-kα radiation (λ-1.54056 Å) in the range of 10–90° with the step size of 0.02°. Using Hitachi S-3000H scanning electron microscope (SEM), the surface morphology of the films were investigated with an accelerating potential of 20 KV. The optical characteristics were studied with the use of a

Table 1 Structural parameters of Gd-doped CdO thin films

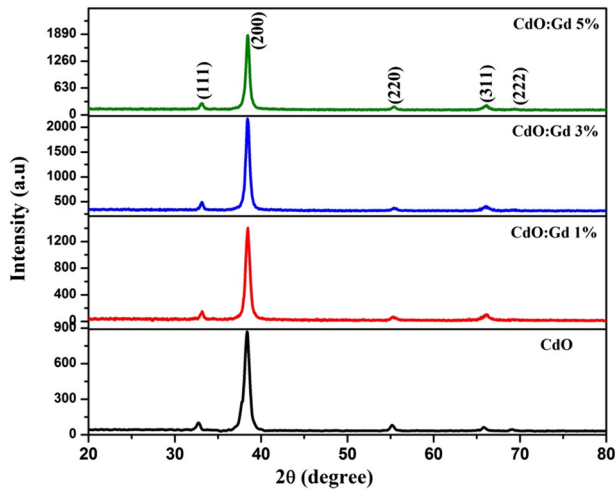| CdO doped with Gd	Thickness (nm)	Lattice const (a) A^0	Crystallite size (nm)	Dislocation density (δ x 10^{15} lines m^{-2})	Strain (ε x 10^{-3} lines^{-2} m^4)	Stacking fault probability	No. of crystallites ×10^{16}	Texture coefficient (TC)
0%	600	4.66428	15	3.93	3.413	1.612	19	3.15
1%	670	4.68312	17	3.41	2.026	1.573	17	3.24
3%	700	4.68346	21	2.18	1.621	1.421	12	3.63
5%	710	4.68414	19	2.76	1.824	1.752	15	3.51

Fig. 1 X-ray diffraction patterns for Gd-doped CdO films

Perkin–Elmer Lambda 35bUV-VIS spectrophotometer. LABRAM-HR model with He-Ne (632.8 nm) laser source was used to record Micro-Raman spectra of prepared films. Horiba JobinYuvan photoluminescence spectroscopy in the wavelength range of 200–800 nm was used to measure the emission properties. A Hall effect set-up at room temperature was used to measure the electrical properties. For the optical illumination of the device, a 200-W halogen lamp was used. To record the photocurrent of the device, a Keithley 4200 semiconductor parameter analyzer was used. Further, a fabricated device of Al/ n-CdO/p-Si/Al that was used for the photoresponse study is presented.

3 Results and discussion

3.1 Structural properties

The structural analysis was carried out by using X-ray diffractometer in the 2θ range from 10 to 90° with Cu-K$_\alpha$ radiation ($\lambda = 1.54056$ Å). Figure 1 shows the X-ray diffractometer profiles of CdO thin films with different Gd-doping concentration (0, 1, 3, and 5%). The obtained XRD pattern is compared with JCPDS card [78–0635], indicating

that the contemporary films are cubic crystal structure of CdO in polycrystalline nature. All the CdO films exhibited one strong orientation along the (200) plane, and the low reflections corresponds to (111), (220), (311), and planes too. The intensity of the (200) peak increased with doping concentration up to 3% and then decreased. The present study indicates that the growth of the film was taken via (200) and it is independent on Gd-doping concentration. However, when the doping concentration was increased up to 3%, the full width at half maximum (β) decreased, indicating better crystallinity and grain size. Similarly, other structural parameters were also calculated along the high-intense (200) peak by using the following relations.

The obtained results well-matched with bulk CdO thin film and lattice parameter $a = 4.683$ Å agreed with the previously reported values [20]. The increase of lattice parameter with doping concentration could attribute to the change of nature, deposition conditions, and the concentration of the inherent imperfections developed in thin films [21]. The dislocation density, microstrain, and the number of crystallites N per unit volume of thin films were determined using the following equations [22–25]:

$$D = \frac{0.9\lambda}{\beta \cos \theta} \tag{1}$$

$$\varepsilon = \frac{\beta \cos \theta}{4} \tag{2}$$

$$\delta = \frac{1}{D^2} \tag{3}$$

The stacking fault probability is a type of defect characterizing the disorders of the prepared CdO thin films. It mainly depends on the position of peaks and it is low along the high-crystallite size in CdO thin films.

The relation connecting stacking fault probability with peak shift $\Delta(2\theta)$ is given by [26]:

$$\alpha = \left[\frac{2\pi^2}{45\sqrt{3}}\right] \left[\frac{\Delta(2\theta)}{\tan \theta_{311}}\right] \tag{4}$$

The number of crystallites (N) per unit volume and dislocation density of different doping concentration of CdO

thin films were calculated using the following equation:

$$N = \frac{t}{D^3} \qquad (5)$$

From Table 1, it could be seen that when the Gd concentration increased to 3% then the strain, dislocation density and the number of crystallites per unit area decreased due to the decrease of crystal defects causing the increase of film quality.

The texture coefficient TC was used to determine the preferred orientation by the following equation [27]:

$$TC\,(hkl) = \frac{I\,(hkl)/I_0(hkl)}{N_{\mathrm{r}}^{-1}\sum I\,(hkl)/I_0(hkl)}. \qquad (6)$$

Here, $I(hkl)$ is the measured intensity of the (hkl) plane, $I_0(hkl)$ is the ASTM standard intensity of the corresponding (hkl) plane, and N is the reflection number of diffraction peaks. The highest TC value was obtained for (200) plane for the prepared nanostructured CdO thin films. The value of the texture coefficient is indicative of the maximum preferred orientation of the films along the diffraction plane. It means that the increase in preferred orientation is associated with the growth in the number of grains along the plane. The stacking fault probability of the CdO thin films mainly consists of peak shift of the predominant orientation of XRD diffraction peak. It was minimum for 3% Gd-doped CdO film.

3.2 Vibrational (FT-IR and FT-Raman) analysis

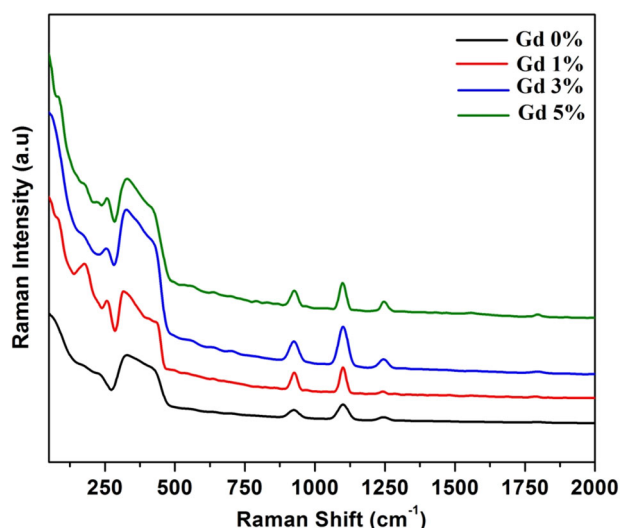It is well known that CdO is mostly Raman inactive; hence its measurement is tough [28]. The Fig. 2 shows the Raman spectra of CdO thin films with different Gd-doping concentration in the range of 200–1200 cm^{-1}. The Raman peak intensity initially increased and then decreased with increasing Gd-doping concentration. In the Gd-doped CdO samples, Raman spectra exhibited a relatively two sharp peaks at 274 and 925 cm^{-1}. It also showed a single broad structure in the range of 300–450 cm^{-1}. Similar data were collected in an earlier study [29]. It was observed that the intensity of the leading peak at 1100 cm^{-1} increased with increasing doping concentration up to 3% Gd. Then, it decreased at higher doping levels. The transverse and longitudinal modes observed in the Raman spectra might have been due to the induced surface effect in the CdO thin films [30, 31]. Another sharp, intense peak at 925 cm^{-1} is also high for present films and indicates that the higher quality of crystal nature was observed in 3% doping concentration, and all the results mentioned in the present study are perfectly matched with the previous results of Sahin et al. [32].

The Fourier transform infrared (FTIR) spectroscopy is the most common technique to identify the chemical bond structure. The FTIR spectrum of pure and different Gd-doped CdO thin films are shown in Fig. 3. The sharp peak at 575 cm^{-1} confirms the bonding of metal–oxygen (Cd-O) [33]. In region 2000–2500 cm^{-1}, very complicated, vibrating, and rotating spectral lines of atmospheric carbon dioxide were obtained. The broad absorption peak around 3400–3600 cm^{-1} is associated to typical polymeric O–H stretching vibration of H$_2$O in CdO lattice [34]. Though the FTIR spectra of all the films appear quite similar with close observation, it is given as there is a minor shift of peaks toward higher wave number with doping concentration that could be occuring due to the incorporation of Gd ions in the Cd crystal lattice.
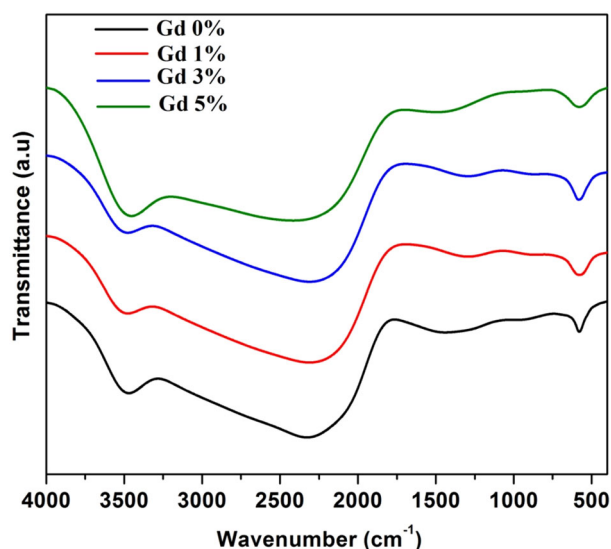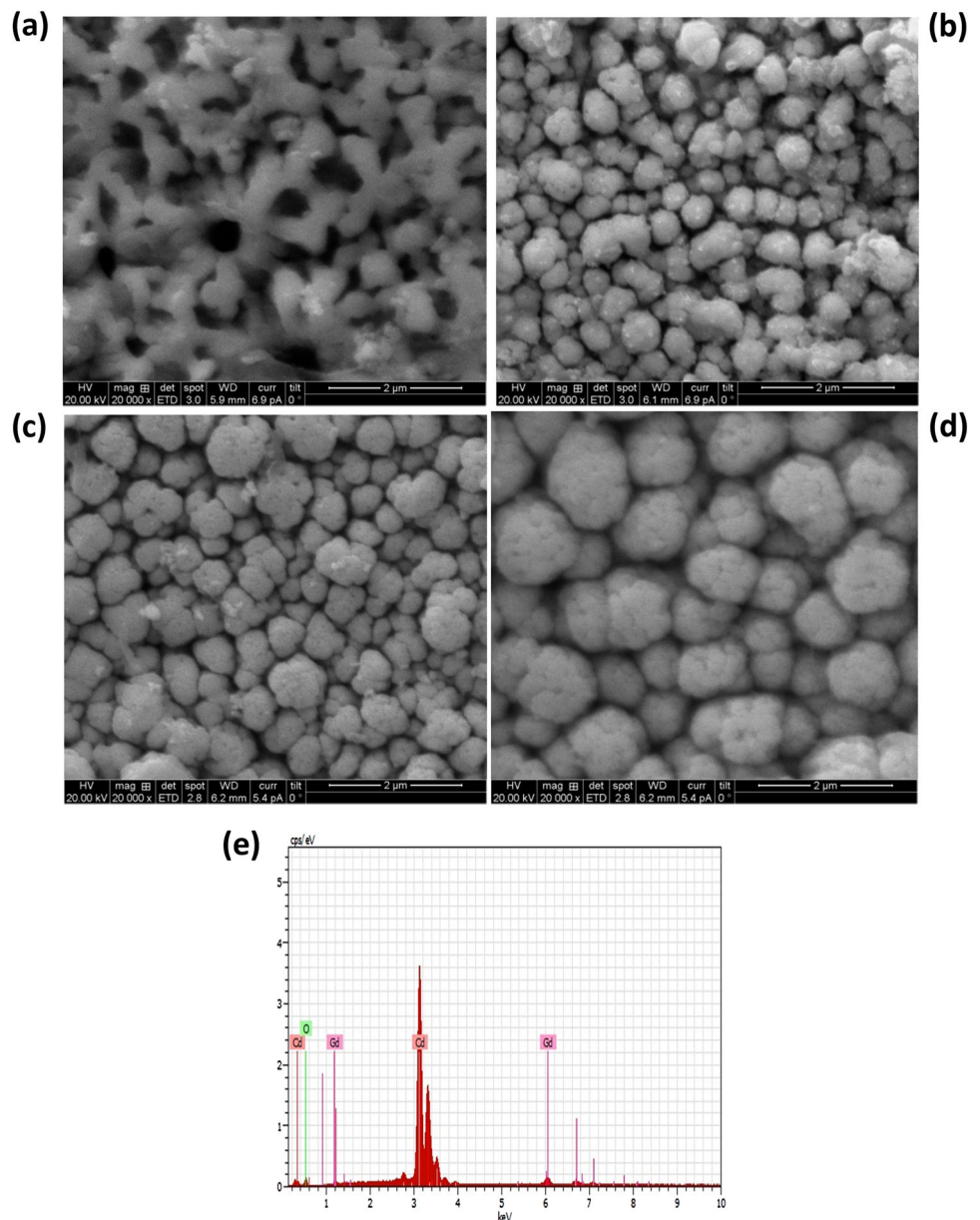
Fig. 2 FT-Raman spectra for Gd-doped CdO films

Fig. 3 FT-IR spectra for Gd-doped CdO films

Fig. 4 SEM micrographs for **a** pure, **b** 1%, **c** 3%, **d** 5% Gd, and **e** EDX spectra for 3% Gd-doped CdO films

3.3 Morphological studies

SEM images of pure and Gd-doped CdO thin films prepared by simple perfume atomizer technique with different Gd-doping concentrations are given in Fig. 4a–d. For all the four samples, SEM photographs were comprised with a magnification of 20,000. The film prepared with pure CdO film showed holes and voids with discontinuities on the surface of the substrate (Fig. 4a), whereas for the films prepared with Gd-doping concentrations (see Fig. 4b–d), it could be visualized that these films exhibited spherical grains without much voids. The well-defined grain boundaries of the film coated with 3% Gd give the shape of cauliflower [35]. The particles were further accumulated by increasing the doping concentration in Fig. 4d. However, the size of the grains increased as the doping concentration was increased with film thickness. Two things—compact distribution over the surface and good connectivity between the grains—were observed in the higher doping concentration of CdO thin films. Such a structure is of great importance due to its high specific surface area and potential applications in many fields [36].

Energy dispersive X-ray spectroscopy was used to carry out elemental analysis of Gd-doped CdO thin films. The EDAX spectrum taken for the CdO thin film deposited with 3% Gd is given in Fig. 4e. The Cd and O ratio of the thin film was close to stoichiometric with previously reported values [36]. It is presumed that this might be due to the

presence of cadmium acetate on the upper surface of the film, which in turn might be due to thermal decomposition. The EDAX results confirm the presence of Cd, O, and Gd in the film.

3.4 Optical properties

The absorption spectra of the deposited CdO thin films with different Gd-doping concentrations are presented in Fig. 5 (a). It is noted that there is high absorption in the UV region and transparent in the visible region. The increase in Gd-doping concentration, the fundamental absorption edge, shows a shift toward the longer wavelengths and lower energies. This sharp fundamental absorption edge corresponds to electron excitation from the valance band to conduction band and it has helped to maintain optical band gap [37]. The obtained absorption edge was similar to other published results of Ghaidia et al. [38]. Optical transmittance spectra of undoped and Gd-doped CdO thin films as a function of wavelength range 400–1100 nm are shown in Fig. 5(b). This plot shows a sharp rise in transmittance near the band edge, which is attributed to the good crystalline nature of the film [39]. The undoped CdO thin film showed high transmittance of 65%, and this value was found to be decreased compared to that in pure, due to increase in thickness with Gd-doping concentration. At lower doping concentration, the transmission is low, and later it starts increasing exponentially with sharp rise in 600–1100 nm region. The lower doping concentration has less transmittance in the visible region when compared with that in the films at higher doping concentration. The increased transmittance might be due to doping concentration.

The direct allowed optical band gap of CdO thin films is determined from the relation between the incident photon energy ($h\nu$) and the absorption coefficient (a) by using the relation [22–25]:

$$ah\nu = B(h\nu - E_g)^n, \tag{7}$$

where E_g and B are optical band gap and constant, respectively. The band gap values depend on crystal structure of the films and the arrangement and distribution of atoms in the crystal lattice. Figure 5(c) shows the variation of band gap values for undoped and Gd-doped CdO thin films. In the present study, the obtained band gap value is 2.42 eV for pure CdO film. Further, the band gap value is raised when adding Gd as the doping element. The observed band gap for doped CdO thin films is found to be in the range of 2.42–2.30 eV and well-matched with the reported values [40, 41]. The band gap values decreased with increase in Gd-doping concentration. The reason for this might be associated due to the change in the crystalline size that might have caused the change in optical band gap [41].
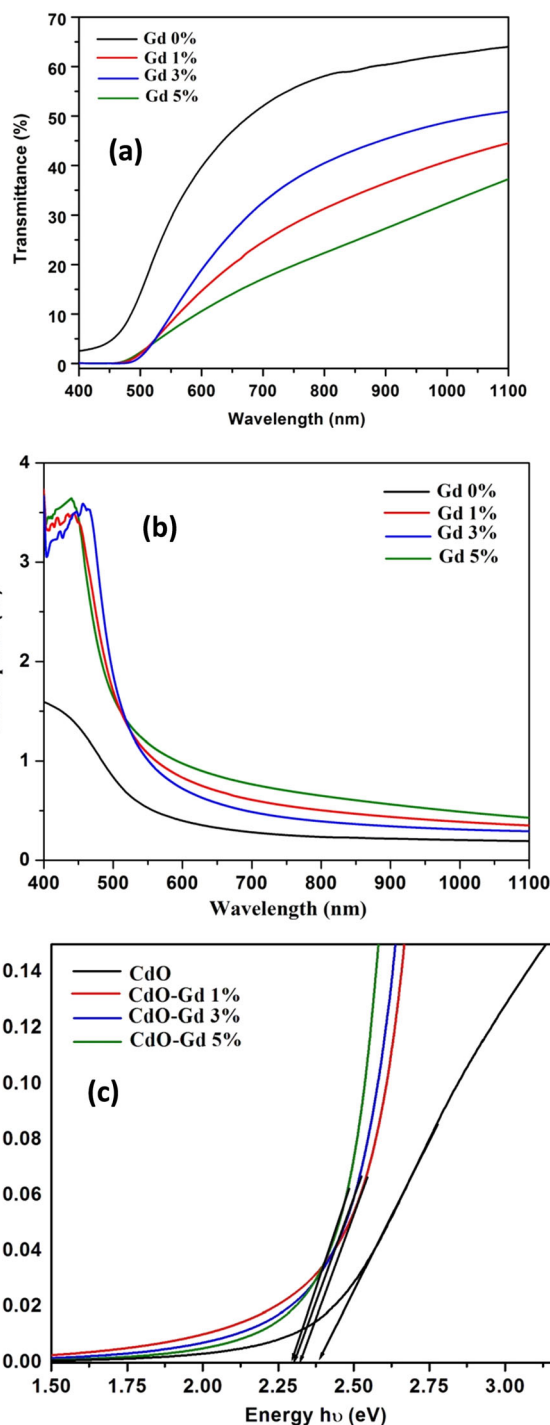

Fig. 5 a Transmittance, b absorbance, and c Tauc's plot for Gd-doped CdO films

3.5 PL studies

PL measurement is a standard technique to observe defects and impurities in semiconductors. The room temperature photoluminescence spectrum of CdO thin film deposited on glass substrate with different Gd-doping concentrations at
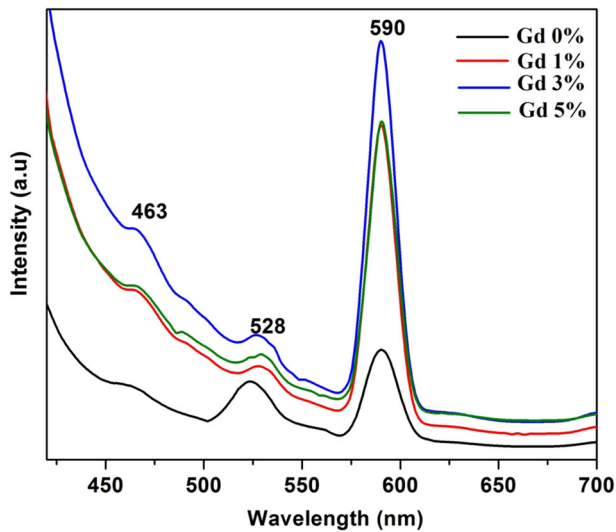
Fig. 6 PL spectra for Gd-doped CdO films

Fig. 7 Carrier concentration (n), hall mobility (μ), and resistivity (ρ) plots for pure and Pr-doped CdO films

Fig. 8 I-V characteristic of 3at% Gd-doped CdO heterostructure

excitation wavelength of 325 nm is recorded in Fig. 6. From the figure it is noticed that the PL emission starts approximately at 460 nm. The PL spectra of all these samples are showing three peaks at 463, 528, and 590 nm that are attributed to visible and green emissions bonds. The observed peak at 528 nm for pure CdO thin film may be ascribed to the deep trap emission and surface-state emission that is less size dependent. Further, this peak is slightly shifted when adding doping element, which is due to the change of band gap. The sharp high intensity of the green emission peak generally originated from the electron–hole recombination at the defect sites due to electron transition from the valence band to conduction band [42]. The green emission peak 590 nm result is perfectly suitable with Sankarasubramanian et al. [43]. Further, improvement in the PL intensity of 3% of Gd is well correlated to the increasing crystallinity as observed from XRD patterns.

3.6 Electrical studies

A four-point probe set-up was used to investigate the electrical studies of the films. The variations of resistivity (ρ), carrier concentration (n), and carrier mobility (μ) of the undoped and Gd-doped CdO thin films are shown in Fig. 7. From these variation, it is observed that the resistivity (ρ) is maximum for the pure CdO thin film. Further, the resistivity values were reduced when adding Gd as the doping element. The resistivity values again decreased with increasing doping concentration up to 3at.%. This may be explained due to the movement of interstitial cadmium atoms from the bulk of the grain to its boundary region [26]. Moreover, increase in resistivity with higher Gd-doping concentration (5at.%) is related to the decrease in free-carrier concentration. This may be associated with the
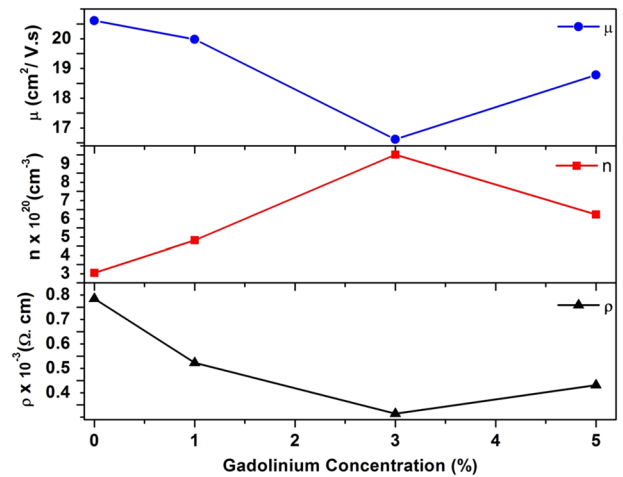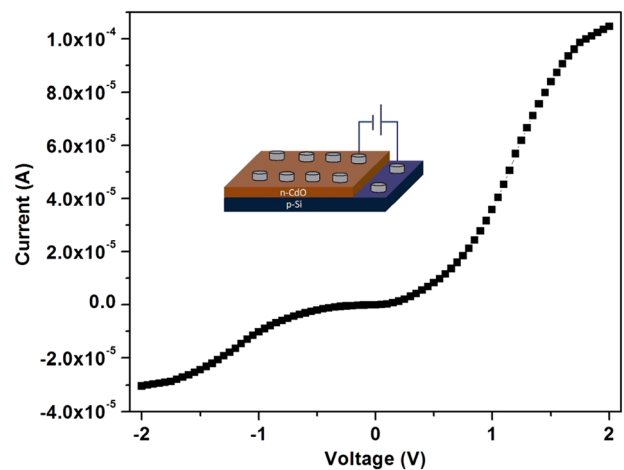
removal of oxygen vacancies and formation of grain boundaries, which act as trap sites for free electrons [44]. However, the films that shows high resistivity at higher doping concentration may be understood from the effect of film thickness. The observed low resistivity (ρ) and high carrier concentration for 3at.% Gd-doped CdO thin film are 3.64×10^{-4} (Ω cm) and 10.2×10^{20} cm^{-3}, respectively. The low-resistivity value is closely matched with other CdO reported values [45].

3.7 Photoresponse studies

Figure 8 shows the room temperature I-V curves of Al/Gd-nCdO/p-Si/Al-based heterojunction diode thin film for 3at.% Gd. The value of the photocurrent density reveals the best photoresponse behavior for the doped CdO thin films.
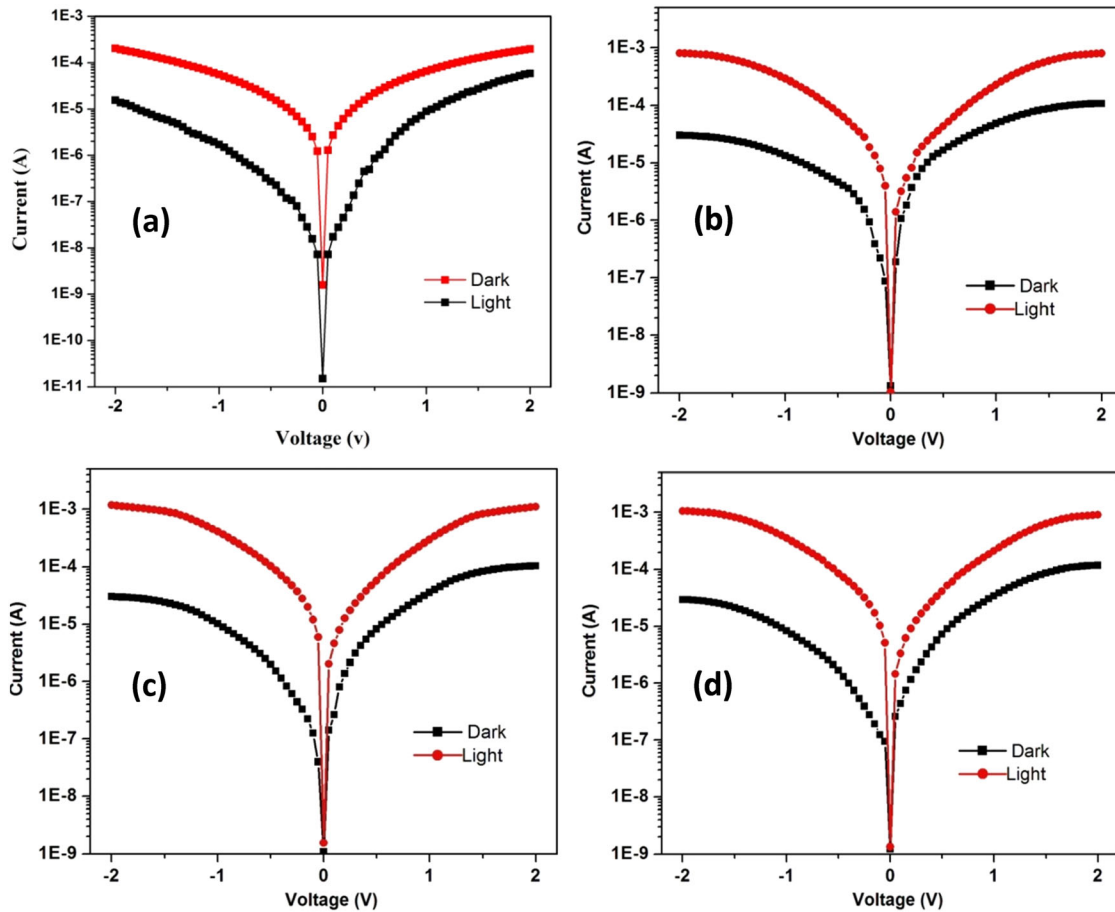
Fig. 9 Forward and reverse current-voltage characteristics of **a** pure, **b** 1%, **c** 3%, and **d** 5% Gd-doped CdO films under dark and illumination

Figure 9a–d shows the forward and reverse current-voltage characteristics of the undoped and doped CdO thin film diodes under dark and illumination conditions. It is clear, from Fig. 9a–d, that the diode was exhibiting an illumination-sensitive behavior. The reverse current is increasing under illumination condition for a given reverse voltage and the observed values are quite higher than the dark values. From this, it is clear that the diode showing a photodiode behavior [46, 47]. It can be observed from I-V plot that reverse current is slightly superior compared to that in the forward one under illumination. Such behavior can be explained as the reduction region of semiconductor separates the photo-generated electron-hole pairs under high electric field. The illumination current increases with increasing doping level as predicted by the thermionic emission (TE) [48]. This increase in current can be attributed to the drift of generated electrons and holes of the host. TE theory defines the current through a Schottky diode as given below [49]:

$$I = I_0 \exp\left(\frac{qV}{nKT} - 1\right), \tag{8}$$

here the symbols are having their usual meanings. The ideality factor (n) and reverse bias saturation current (I_o) are calculated through equations [50]:

$$n = \frac{q}{KT}\frac{dV}{d(InI)} \tag{9}$$

$$\phi_b = \frac{KT}{q} In\left(AA^* T^2 / I_0\right), \tag{10}$$

here all the used symbols are commonly used and have usual meanings. We have measured the current in reversible mode up to 2 V from 0 (see Figs. 8, 9). Turn-on voltage for the fabricated heterojunction is obtained about ~0.43 V, which shows the constructive retort to light [51]. The semi-logarithmic curve of the device revealed that the characteristics with the slope of linear region of the forward bias in I-V curves. This enables to evaluate the value of (n) and observed to be 4.31 using Eq. (9) (see Table 2). It is known that this value should be unity for an ideal diode; however, we have observed higher value that may be due to interface states, non-uniform film deposition, and series resistance. The y-intercept of semi-logarithmic curve give the value of

Table 2 Variations of photoresponse of undoped and Gd-doped CdO thin films

CdO doped with Gd (%)	Potential barrier ($\varnothing_b$) (eV)	Ideality factor (n)	Photo responsivity (R) mA/W	Quantum efficiency (QE) %
0	0.73	4.57	182	37.82
1	0.72	4.49	225	53.72
3	0.70	4.31	365	76.64
5	0.75	6.50	334	70.22

I_o around 6.7034×10^{-7} Å. The value of $\varnothing_b$ is calculated around 0.70 eV for 3at.% Gd-doped film using Eq. (10) (see Table 2). It can be seen that the value of photocurrent enriched up to a certain level under illumination as during this the number of free-charge carriers increase. This indicates that the constructed device have photo-conducting nature. Moreover, the responsivity (R) is determined using the equation below [52]:

$$R = \frac{I_{ph}}{PA}, \tag{11}$$

here I_{ph} is current in illumination, P is irradiation of lamp, and A is area of diode. The value of the R of Al/Gd-nCdO/p-Si/Al hybrid heterojunction diode is found to be 365 mA/W at a bias of 2 V (see Table 2).

The equation for quantum efficiency (QE) is calculated as in the following equation [53]:

$$QE = \frac{Rhc}{q\lambda}, \tag{12}$$

where R is the responsivity of the diode, h is the planck's constant, c is the velocity of light, q is the charge of an electron, and λ is the wavelength of the source light. The higher value of the QE of p-Si/n-CdO (Gd3%) hybrid heterojunctions was found to be 76.64% at a bias of 2 V.

4 Conclusion

In summary, we have successfully prepared undoped and doped CdO thin films by spray pyrolysis using perfume atomizer on glass and silicon substrates. Influence of Gd doping on key properties of CdO thin films were studied. XRD spectra indicate the polycrystalline nature of the deposited films. It is clear that the morphology of the CdO thin films is influenced by Gd doping revealed by SEM. The Energy dispersive X-ray spectroscopy spectra confirmed the presence of gadolinium in this composition and CdO structure. The band gap values decreased with increasing doping concentration and was found in the range of 2.42–2.30 eV. PL studies confirm that the films exhibit strong luminescent properties. From the Hall Effect studies, the low electrical resistivity value $3.64 \times 10^{-4}\,\Omega\,cm$ and

high carrier concentration value $10.2 \times 10^{20}\,cm^{-3}$ are obtained for 3at.% Gd content. The Al/Gd-nCdO/p-Si/Al heterojunction-based photodiodes were prepared and the obtained responsivity and QE were found to be 365 mA/W and 76.64%, respectively, for 3at.% Gd. Hence, the Gd: CdO films acts as potential candidate as heterojunction photodiode for application in optoelectronic devices.

Compliance with ethical standards

Conflict of interest The authors declare that they have no competing interests.

References

1. Obaid AS, Mahdi MA, Ramizy A, Hassan Z (2012) Adv Mater Res 364:60–64
2. Ferroand R, Rodriguez JA (2000) Sol Energy Mater Sol Cells 64:363–370
3. Serpetci Z, Gunduz B, Al-Ghamdi AA, Al-Hazmic F, Arik K, ElTantawy F, Yakuphanogly F, Farooq WA (2014) Acta Phys Pol A 126:20–25
4. Minami T, Ida S, Miyata T (2002) Thin Solid Films 416:92–96
5. Zhao Z, Morel DL, Ferekides CS (2002) Thin Solid Films 413:203–211
6. AzizarRahman M, Khan MKR (2014) Mater Sci Semicond Process 24:26–33
7. Gupta RK, Ghose K, Patel R, Mishra SR, Kahol PK (2008) Mater Lett 62:3373–3375
8. Yahia IS, Salem GF, Abd El-sadek MS, Yakuphanoglu F (2013) Superlattices Microstruct 64:178–184
9. Deokate RJ, Salunkhe SV, Agawane GL, Pawar BS, Pawar SM, Rajpure KY, Moholkar AV, Kim JM (2010) J Alloys Compd 496:357–363
10. Sankarasubramanian K, Soundararajan P, Logu T, Kiruthiga S, Sethuraman K, Ramesh R (2014) babu and K. Ramamurthi. Mater Sci Semicond Process 26:346–353
11. Gupta RK, Ghosh K, Patel R, Kahol PK (2011) J Alloys Compd 509:4146–4149
12. Dakhel AA, Ali-Mohamed AY (2010) J Sol-Gel Sci Technol 55:348–353
13. Pan LL, Li GY, Lian JS (2013) Appl Surf Sci 274:365–370
14. Dakhel AA (2010) Thin Solid Films 518:1712–1715
15. Ferro R, Rodriguez JA, Vigil O, Morales-Acevedo A (2001) Mater Sci Eng B 87:83–86
16. de Leon-Gutierrez LR, Cayente-Romero. JJ, Peza-Tapia JM, Barrera-Calva E, Martinez-Flores JC, Ortega-Lopez M (2006) Mater Lett 60:3866–3870
17. Usharani K, Raja N, Manjula N, Nagarethinam VS, Balu AR (2015) Int J Thin Films Sci Technol 42:89–96
18. Dakhel AA (2011) Mater Chem Phys 130:398–402
19. Deva Arun Kumar K, Valanarasu S, Tamilnayagam V, Amalraj L (2017) J Mater Sci Mater Electron 1–8. https://doi.org/10.1007/s10854-017-7278-7
20. Thiruramanaathan P, Hikku GS, Krishna Sharma R, Amalraj L (2015) Mater Focus 4:17

21. Gurumurugan K, Mangalaraj D, Narayandass SaK (1995) J Cryst Growth 147:355–360

22. Shkir Mohd, Kilany M, Yahia IS (2017) Ceram Int 43:14923–14931

23. Shkir Mohd, AlFaify S, Ganesh V, Yahia IS (2017) Solid State Sci 70:81–85

24. Shkir M, AlFaify S, Yahia IS, Ganesh V, Shoukry H (2017) Phys B Condens Matter 508:41–46

25. Shkir M, Yahia IS, Ganesh V, Algarni H, AlFaify S (2017) Mater Lett 176:135–138

26. Usharani K, Balu AR, Suganya M, Nagarethinam VS (2015) J Appl Chem Res 9:47–63

27. Mariappan R, Ragavendar M, Ponnuswamy V (2011) J Alloys Compd 509:7337–7343

28. Rafa MA, Rousdy N (2010) Philos Mag Lett 90:113–120

29. Popovic ZV, Stanisic G, stojanovic D, Kostic R (1991) Phys Status Solidi B 165:109–112

30. Cusco R, Ibanez J, Domenech-Amador N, Artus L, Zuniga-Perez J, Munoz Sanjose V (2010) J Appl Phys 107:063519

31. Thema FT, Beukes P, Gurib-Fakim A, Maaza M (2015) J Alloys Compd 646:1043–1048

32. Sahin B (2013) Sci World J 2013:1–5

33. Knaepen E, Mullens J, Yperman J, Poucke LCV (1996) Thermochim Acta 284:213–227

34. Thirumoorthi M, Thomas Joseph Prakash J (2015) J Asian Ceram Soc 191:2187–0764

35. Ren HX, Huang XJ, Yarimaga O, Choi YK, Gu N (2009) J Colloid Interface Sci 334:103–107

36. K Usharani AR Balu (2014) The Chinese society for metals and Springer-Verlag Berlin Heidelberg

37. Joseph Edison D, Nirmala W, Kumar KDA, Valanarasu S, Ganesh V, Shkir Mohd, AlFaify S (2017) Phys B Condens Matter 523:31–38

38. Salman G, Kareem E, Naje AN (2014) Int J Innovative Sci Eng Technol 1:147–152

39. Al-Sabayleh MA (2008) Al-Qura Univ J Sci Med Eng 20:17–30

40. Afify HH, Ahmed NM, Tadros MY, Ibrahim FM (2014) J Electr Syst Infor Technol 1:119–128

41. Dakhel AA (2009) Opt Mater 31:691–695

42. Mitra A, Thareja RK (2001) Photoluminescence and ultraviolet emissions from nano crystalline ZnO thin films. J Appl Phys 89:2025–2028

43. Sankarasubramanian K, Soundarrajan P, Sethuraman K, Ramesh Babu R, Ramamurthi K (2014) Superlattices Microstruct 69:29–37

44. Kim IH, Ko JH, Kim D, Lee KS, Lee TS, Jeong JH, Cheong B, Back YJ, Kim WM (2006) Thin Solid Films 515:2475–2480

45. Karakaya S, Ozbas O (2014) Usak Univ J Mater Sci 2:159–164

46. Tataroglu A, Tuncer H, Al-Ghamdi AA, Dere A, Arif B, Yol S, Ozdemir N, El-Tantawy F, Yakuphanoglu F (2015) Synth Metals 206:15–23

47. Tataroglu A, Al-Ghamdi AA, Bin Omran S, Farooq WA, El-Tantawy F, Yakuphanoglu F (2014) J Sol-Gel Sci Technol 71:421–427

48. Schwede JW, Bargatin I, Riley DC, Hardin BE, Rosenthal SJ, Sun Y, Schmitt F, Pianetta P, Howe RT (2010) Nat Mater 9:762–767

49. Rhoderick EH, williams RH (1988) Metal-semiconductor contacts, 2nd edn. Clarendon Press, Oxford

50. Ugurel SAE, Serifoglu K, Turut A (2008) Microelectron Eng 85:2299–2303

51. Chen P, Ma X, Yang D (2007) J Appl Phys 101:053103

52. Naderi N, Hashim MR (2013) J Alloys Compd 552:356–362

53. Tatar B, Demiroglu D, Urgen M (2014) Investigation of structural and electrical properties of p-CuPc/c-Si and p-CuPc/a-Si/c-Si hybrid photodiodes prepared by CSP technique. Microelectron Eng 126:184–190